International Journal of Heat and Mass Transfer 251 (2025) 127408

Contents lists available at ScienceDirect

International Journal of Heat and Mass Transfer

journal homepage: www.elsevier.com/locate/ijhmt

Impact of cross-section geometry on microchannel heat sink performance in the presence of slip and temperature jump boundary conditions

Pamela Vocale [a,*], Gian Luca Morini [b]

[a] Department of Engineering and Architecture, University of Parma, Parco Area delle Scienze 181/A, 43124 Parma, Italy
[b] DIN – Alma Mater Studiorum Università di Bologna, Viale Risorgimento 3, 40135 Bologna, Italy

ARTICLE INFO

Keywords:
Slip boundary conditions
Superhydrophobic walls
Rarefied gas
Microchannels heat sink

ABSTRACT

The geometry of microchannels plays a crucial role in determining the heat transfer efficiency and pressure drop in microchannel heat sinks. The choice of channel shape is often guided by practical factors, such as manufacturability, system integration, and cost-effectiveness. This study aims to evaluate the thermohydraulic performance of laminar flow in microchannels with various cross-sectional geometries, including rectangular, trapezoidal, double-trapezoidal, elliptical and rhombic shapes. This analysis considers the effects of slip velocity and temperature jump at the channel walls, as to date, research on the thermal characterization of microchannels operating in the slip flow regime – particularly those with hydrophobic or superhydrophobic surfaces – remains limited. The heat transfer problem is addressed by assuming a constant heat transfer rate along the axial direction of the channel walls with a uniform temperature distribution around the perimeter of the cross-section. This condition is particularly relevant for microchannels subjected to an imposed heat flux, especially when the channel walls are constructed from materials with high thermal conductivity. The numerical results reveal that rectangular and double-trapezoidal (hexagonal) cross-sections demonstrate the highest thermohydraulic performance, whereas the rhombic cross-section performs the worst. Moreover, the outcomes presented here highlight that the rhombic geometry is the most sensitive to slip effects, while the double-trapezoidal geometry is the least sensitive.

1. Introduction

Microchannel heat exchangers are used in several fields, including microelectronic cooling, aerospace, biomedical processes, and the automotive industry [1]. The shape of microchannels is one of the key factors influencing the heat transfer capability and pressure drop in microchannel heat sinks (MCHSs) [2]. The cross-sectional shape of the channel can impact flow behavior and induce secondary flow due to shear stress, which in turn affects both heat transfer and pressure drop [3]. The selection of channel shape is often influenced by practical considerations, such as manufacturability, integration with larger systems, and cost. For instance, although circular microchannels may provide superior flow characteristics, they are more difficult to produce using methods like lithography, which more readily accommodate rectangular and trapezoidal shapes.

Numerous researchers have explored the impact of channel shape on the thermohydraulic performance of MCHSs, as emphasized in a recent review by Dong et al. [2].

Chen et al. [4] numerically investigated the fluid flow and heat transfer in triangular, rectangular, and trapezoidal microchannel heat sinks. Their results revealed that MCHSs with a triangular cross-section exhibited the highest thermal efficiency, whereas those with a rectangular cross-section exhibited the lowest (i.e., the thermal efficiency in [3] was defined as the ratio between the heat transfer rate and the pumping power).

Gunasegaran et al. [5] conducted a numerical investigation of the impact of various geometrical parameters on the heat transfer characteristics of MCHSs. Their results indicated that MCHSs with rectangular cross-section exhibited the highest heat transfer coefficient and Poiseuille number, while triangular microchannels showed the lowest values. Trapezoidal microchannels fell in between.

Canhoto and Reis [6] investigated the optimization of a heat sink consisting of parallel ducts with circular, parallel plates, rectangular, square, and equilateral triangle cross-sections enclosed within a finite volume and operating under a fixed pumping power to achieve maximum heat transfer density. The results of the optimization were

* Corresponding author.
E-mail address: pamela.vocale@unipr.it (P. Vocale).

https://doi.org/10.1016/j.ijheatmasstransfer.2025.127408
Received 8 April 2025; Received in revised form 9 June 2025; Accepted 9 June 2025
Available online 13 June 2025

further extended to the scenario in which the objective was to minimize pumping power while maintaining a fixed heat transfer density.

Salimpour et al. [7] demonstrated through theoretical analysis and numerical simulations that microchannel heat sinks with rectangular, elliptical, and isosceles triangular cross-sections have an optimal hydraulic diameter at which global thermal conductance reaches its maximum.

Alfaryjat et al. [8] numerically studied the thermohydraulic performance of MCHSs with several aspect ratios, comparing different shapes (i.e., hexagonal, circular, and rhombic microchannels). They found that the circular shape exhibited a better temperature distribution, with a higher top wall temperature compared to other shapes. Additionally, the hexagonal shape had the highest heat transfer coefficient, while the circular shape had the lowest pressure drop.

Wang et al. [9] conducted a numerical investigation on the performance of rectangular, trapezoidal, and triangular cross-sectional shaped MCHSs. Their findings highlight that the rectangular microchannel exhibits the lowest thermal resistance, followed by the trapezoidal and triangular microchannels.

Jing and He [10] numerically studied fluid flow and heat transfer in microchannels with three cross-sections (i.e., elliptical, rectangular, and triangular). They found that at the same hydraulic diameter, the triangular-shaped microchannel exhibited the lowest hydraulic resistance and the smallest convective heat transfer coefficient. On the other hand, their numerical results revealed that for elliptical and rectangular microchannels, there exists a critical hydraulic diameter at which their hydraulic resistances are equal. When the hydraulic diameter is smaller than this critical value, the elliptical microchannel exhibits lower hydraulic resistance; when it is larger, the rectangular microchannel has the advantage.

From the literature survey above, it can be observed that the thermohydraulic performance of microchannel heat sinks can be enhanced by modifying the channel aspect ratio and the cross-sectional shape of the microchannels. Moreover, the literature review points out that in all works dealing with the analysis of the influence of the channel shape on the thermohydraulic performance of microchannel heat sinks or heat exchangers, the effects of velocity slip were disregarded.

Slip flow close to the solid channel walls can be observed under specific operating conditions, such as when liquids flow in microchannels with superhydrophobic walls [11,12] or when the working fluid is a rarefied gas [13]. Moreover, slip has also been observed over rough and porous microchannel walls [14,15].

When rarefied gas flows through a microchannel, the convective heat transfer coefficients are typically low. However, the presence of slip flow and temperature jump at the solid walls could lead to a slight increase in the overall heat transfer coefficient in microchannel heat sinks. This enhancement is influenced by the surface properties of the walls, specifically through the dynamic and thermal accommodation coefficients [13].

On the contrary, it has been demonstrated how, in the presence of liquid flows, the use of superhydrophobic walls in a microchannel heat sink is able to reduce the frictional resistance of liquid, significantly decreasing the total pressure drop. This effect is due to the reduction in the contact area between the channel walls and the flowing liquid. For liquids flowing in channels having conventional wall surfaces, no-slip velocity and temperature continuity at the interface are usually assumed. In contrast, in microchannels with hydrophobic walls, velocity slip and temperature jump conditions at the interface must be taken into account.

Although the specific operating conditions for slip flow depend on the fluid type fluid (gas or liquid), the analysis can be performed using a unified boundary condition that accounts for both slip velocity and temperature jump at the solid walls (Fig. 1). Consequently, the mathematical model employed in this study is applicable for analyzing the behavior of both gases and liquids.

Research on the thermohydraulic performance of microchannels with hydrophobic and superhydrophobic surfaces has been relatively scarce.

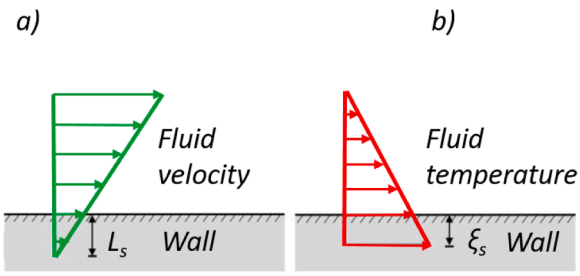

Fig. 1. Schematic of slip flow: a) velocity slip; b) temperature jump.

Hajmohammadi et al. [16] presented a numerical investigation aimed at finding the optimal geometric design of microchannel heat sinks with rectangular channels by considering both slip and no-slip boundary conditions. They found that the slip boundary condition significantly impacted the performance of MCHS and the optimal geometrical parameters. For instance, their numerical results revealed that as the slip parameter increased, the optimal aspect ratio of rectangular microchannels became larger, resulting in narrower microchannels compared to the no-slip scenario.

Ermagan and Rafee [17] numerically investigated the performance of a wavy microchannel heat sink with superhydrophobic walls. Their findings reveal that using superhydrophobic walls leads to a reduction in both friction factor and Nusselt number compared to conventional walls. However, the decrease in pressure drop outweighs the reduction in convective heat transfer, resulting in an overall improvement in heat sink performance. Nevertheless, the advantage of superhydrophobic walls diminishes as channel waviness increases. Moreover, Ermagan and Rafee [18] demonstrated the influence of wall hydrophobicity on the optimal geometric parameters of MCHS. The same authors [19] also studied the impact of pumping power on the optimal geometric parameters of converging microchannels with superhydrophobic walls integrated into a heat sink.

Gong et al. [20] investigated fluid flow and heat transfer in microtubes under slip flow conditions by considering a fully developed laminar flow. Their results showed that the Poiseuille number (defined as the friction factor-Reynolds number product) decreases while the Nusselt number increases as the ratio of slip length to tube radius increases. Moreover, they developed correlations for the Poiseuille number and the Nusselt number as a function of the ratio of slip length to tube radius.

A complete comparative analysis of the influence of the channel shape on the thermohydraulic performance of the microchannel heat sinks or heat exchangers when working fluid works in a slip flow regime has not yet been carried out, at least to the best of the author's knowledge. Therefore, the main objective of this study was to compare the thermohydraulic performance of laminar flows in microchannels characterized by rectangular, trapezoidal, double-trapezoidal, elliptical, and rhombic cross-sections by emphasizing the effect of the presence of slip velocity and temperature jump at the wall on the optimal thermohydraulic performance of microchannel heat sinks.

The selection of the microchannel cross-sectional geometries investigated in this study is informed by the most commonly employed microfabrication techniques for micro heat sinks. Rectangular cross sections are widely adopted due to their relative ease of fabrication through various methods, including 3D printing, micro laser cutting, and chemical etching [21]. Elliptical cross sections can be realized using LIGA, die cutting, and 3D printing [22]. More complex geometries, such as trapezoidal, double-trapezoidal, and rhombic cross-sections, are typically fabricated via anisotropic chemical etching on ⟨100⟩ silicon wafers [23], wherein the apex angle is inherently fixed at 54.74° as a result of the crystalline orientation of silicon. Nonetheless, when these

geometries are produced using additive manufacturing techniques, such as 3D printing, the apex angle can vary, thereby enabling greater flexibility in design and optimization [24].

2. Numerical analysis

2.1. Governing equations and boundary conditions

In the study presented here, a fully developed laminar flow in parallel microchannels, such as those found in MCHS (see Fig. 2a), was investigated. The fluid flowed in microchannels with rectangular, trapezoidal, double-trapezoidal (or hexagonal), elliptical, and rhombic cross-sections (see Fig. 2b). Each geometry was characterized by an aspect ratio $\gamma = H_{ch}/W_{ch}$, where W_{ch} represents the maximum width of the cross-section, while H_{ch} denotes its height. A Cartesian coordinate system was used with the origin positioned at the center of the cross-section (see Fig. 2a).

To address the fluid flow and heat transfer problems in microchannels characterized by different cross-section geometries, the following assumptions were made: the fluid is Newtonian, incompressible, and with constant properties, and the flow is fully developed and in steady-state conditions. It is important to note that for a gas to be treated as incompressible, its Mach number must be <0.3 [25].

Given these assumptions, the momentum and energy equations can be written as follows:

$$\mu\left(\frac{\partial^2 v}{\partial x^2}+\frac{d^2 v}{dy^2}\right)=\frac{\partial p}{\partial z} \tag{1}$$

$$\rho c_p v\frac{\partial T}{\partial z}=\lambda\left(\frac{\partial^2 T}{\partial x^2}+\frac{\partial^2 T}{\partial y^2}\right) \tag{2}$$

where μ, ρ, c_p, and λ are the fluid dynamic viscosity, density, specific heat at constant pressure, and thermal conductivity, respectively, and p, v and T are the fluid pressure, velocity, and temperature, respectively.

The non-dimensional forms of the momentum and energy equations were derived to characterize the flow and heat transfer behavior in microchannels, as shown in Eqs. (3) and (4), respectively.

$$\frac{\partial^{*2} v^*}{\partial x^{*2}}+\frac{\partial^{*2} v^*}{\partial y^{*2}}+p^*=0 \tag{3}$$

$$\frac{\partial^{*2} T^*}{\partial x^{*2}}+\frac{\partial^{*2} T^*}{\partial y^{*2}}=\frac{v^*}{A^*} \tag{4}$$

where the following non-dimensional quantities were considered:

$$x^*=\frac{x}{D_h},\ y^*=\frac{y}{D_h},\ v^*=\frac{v}{\bar{v}},\ T^*=\frac{\lambda(T-T_w)}{q' D_h},\ p^*=-\frac{D_h^2}{\mu\bar{v}}\frac{dp}{dz},\ A^*=\frac{A}{D_h^2} \tag{5}$$

In Eq. (5) D_h is the hydraulic diameter of the microchannel, $\bar{v}$ is the average fluid velocity, q' is the thermal power per unit of length, and A denotes the area of the cross-section.

The momentum equation in the non-dimensional form was solved by considering the first model for the slip velocity presented by Navier [26]:

$$u^*|_w = L_S^*\left.\frac{\partial u^*}{\partial n^*}\right|_w \tag{6}$$

where $u^*|_w$ represents the non-dimensional velocity of the fluid near the walls, L_S^* is the non-dimensional slip length (i.e., $L_S^*=\frac{L_s}{D_h}$ being L_s the slip length), and n^* indicates the non-dimensional normal to the wall. The subscript w indicates the wall.

For fluids in microchannels with superhydrophobic walls, the slip length primarily depends on the texture pitch, the cavity fraction, the hydraulic diameter, and the Reynolds number [12,17,18]. It can be evaluated from experimental data and numerical investigations [1, 27–30].

For gases in microchannels, the slip length depends on the gas–surface interaction and the Knudsen number (defined as the ratio between the characteristic dimension of the microchannel and the gas mean free path [13]).

The non-dimensional energy equation was solved using the H1 boundary condition, where the heat transfer rate through the wall remains constant along the axial direction, while the wall temperature remains uniform around the perimeter [31]). This thermal boundary condition is especially useful for microchannels with an imposed heat flux when solid walls are made of high thermal conductivity materials.

In addition, when the channel walls are hydrophobic or the working fluid is a rarefied gas, the temperature jump due to surface coating or rarefaction can be imposed as follows:

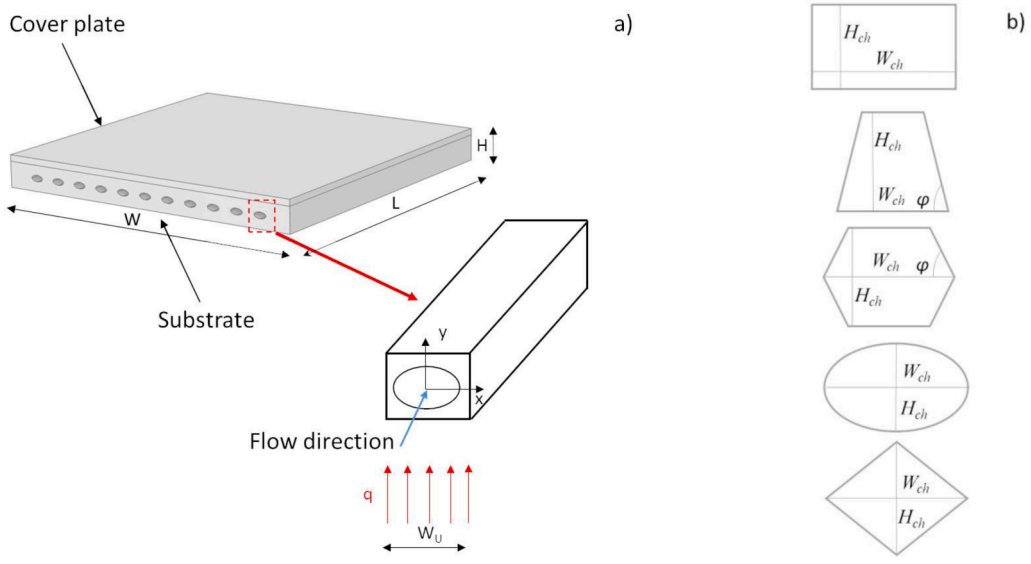

Fig. 2. Micro heat sinks investigated in the present study: a) Schematic views; b) considered cross-sections. W_{ch} and H_{ch} represent the maximum width and the height of the cross-section, respectively; φ denotes the apex angle for trapezoidal and double-trapezoidal microchannels.

$$T^*|_w = \xi_S^* \left.\frac{\partial T^*}{\partial n^*}\right|_w \tag{7}$$

where $T^*|_w$ represents the fluid temperature at the wall and ξ_S^* is the non-dimensional temperature jump coefficient (i.e., $\xi_S^* = \frac{\xi_s}{D_h}$ where ξ_s is the temperature jump coefficient).

The temperature jump coefficient depends on the texture pitch, the cavity fraction, and the hydraulic diameter [12,17,18] for fluids in microchannels with hydrophobic walls, while it depends on the gas–surface interaction, the Prandtl number, the specific heat ratio, and the Knudsen number for gases in microchannels with traditional walls [13].

The average Nusselt number for all cross-section shapes was evaluated as follows:

$$Nu = \frac{hD_h}{\lambda} = -\frac{1}{P^* T_b^*} \tag{8}$$

where h indicates the average convective heat transfer coefficient, T^*_b represents the fluid bulk temperature in the non-dimensional form, and P^* the non-dimensional perimeter of the cross-section (i.e., $P^* = \frac{P}{D_h}$ where P is the perimeter of the cross-section).

The dimensionless fluid bulk temperature was evaluated as follows:

$$T_b^* = \frac{1}{A^*}\int_{A^*} v^* T^* \; dA^* \tag{9}$$

The Poiseuille number, which was defined as the Fanning friction factor-Reynolds number product, was calculated using the following equation:

$$fRe = -\frac{dp}{dz}\frac{2D_h}{\rho \bar{v}^2}\frac{\rho \bar{v} D_h}{\mu} = -\frac{1}{2}\frac{D_h^2}{\mu \bar{v}}\frac{dp}{dz} = -\frac{p^*}{2} \tag{10}$$

To evaluate the impact of slip effects on the thermohydraulic performance of the MCHS, the total thermal resistance and pumping power were evaluated.

The total thermal resistance was expressed as illustrated in [32]:

$$R_{tot} = R_{cond} + R_{conv} + R_f =$$

$$= R_{cond} + \frac{1}{hA_{conv}} + \frac{1}{\rho \dot{V} c_p} \tag{11}$$

where R_{cond}, R_{conv} and R_f are the conductive, convective, and fluid thermal resistance, respectively; A_{conv} indicates the convective heat transfer area (i.e., $A_{conv} = PL$ with L the length of the MHCS) and $\dot{V}$ is the volumetric flow rate ($A\bar{v}$).

By scaling the thermal resistances with $R_0 = \left(\frac{1}{\lambda D_h}\right)$ it was possible to write Eq. (11) in a dimensionless form:

$$R_{tot}^* = R_{cond}^* + R_{conv}^* + R_f^*$$

$$= \frac{R_{cond}}{\left(\frac{1}{\lambda D_h}\right)} + \frac{\frac{1}{hA_{conv}}}{\left(\frac{1}{\lambda D_h}\right)} + \frac{\frac{1}{\rho \dot{V} c_p}}{\left(\frac{1}{\lambda D_h}\right)} = R_{cond}^* + \frac{1}{NuP^*L^*} + \frac{1}{A^* Pe} \tag{12}$$

where $L^* = \frac{L}{D_h}$ and Pe is the Peclet number (i.e., $Pe = RePr$).

The pumping power was evaluated as follows [18,20]:

$$\Omega = \dot{V}\Delta p \tag{13}$$

where Δp indicates the pressure drop.

Eq. (13) was written in dimensionless form as follows:

$$\Omega^* = \frac{\Omega}{\mu L \bar{v}^2} = -A^* p^* = 2fReA^* \tag{14}$$

To optimize the thermohydraulic performance of the heat sinks, a dimensionless function was introduced, defined as the inverse of the product of dimensionless pumping power and dimensionless convective thermal resistance:

$$\Phi^* = \frac{1}{R_{conv}^* \Omega^*} = \frac{1}{\frac{1}{NuP^*L^*} 2fReA^*} = 2L^* \frac{Nu}{fRe} \tag{15}$$

It is evident that a key parameter for optimizing the thermohydraulic performance of the heat sinks is the ratio of the Nusselt number to the Poiseuille number given a fixed channel length (L).

The ratio between the Nusselt number and the Poiseuille number was also adopted by Ermagan and Rafee [17] to assess the performance of wavy microchannels with superhydrophobic walls. It is important to highlight that in [17], this ratio was defined as the goodness factor, although the original definition by Shah and London [31] also included the Prandtl number.

The mathematical model represented by Eqs. (3) and (4) was implemented in COMSOL Multiphysics® and solved using its equation-based modeling tools. The solver was configured with a relative tolerance of 10^{-6}. Quadratic shape functions were used for both the fluid velocity and temperature fields, given the low flow velocities involved [33].

2.2. Mesh convergence analysis and model validation

To numerically analyze the thermohydraulic performance of microchannels, a grid independence study was first conducted for each cross-section. The microchannels were meshed using triangular elements. For each cross-section, five different mesh sizes were considered. Special attention was given to ensuring a sufficient number of elements in the corners of the microchannel, where high temperature gradients were expected.

Microchannels with a small aspect ratio are selected as a representative case to illustrate the results of mesh independence analysis. In Fig. 3, the results in terms of Nusselt number are presented as a function of the total number of elements N.

It can be observed that the difference between the mesh characterized by the lowest value of N and that characterized by the highest value of N is in general very small (i.e., the maximum difference for the Nusselt number was <1 %). Given the small computational effort required for meshes characterized by a number of elements higher than 1000, these configurations were chosen for further analysis.

The accuracy of the model was validated by comparing it with the data available in the existing scientific literature. Specifically, numerical findings for elliptical microchannels in the slip flow regime (Fig. 4a) were compared with the analytical solutions of Su et al. [34], while numerical outcomes for rectangular microchannels in the slip flow regime (Fig. 4b) were compared with the results obtained using the analytical solution of Ghodoossi and Eğrican [35]. For both cross-sectional shapes, perfect agreement was observed across aspect ratio values considered in this study.

The numerical outcomes for trapezoidal microchannels with $\varphi = 30°$ and $\varphi = 60°$ were compared with the experimental data from Kewalramani et al. [36] in terms of the Nusselt number in the continuum flow regime ($L^*_s = 0$). It is important to highlight that in [36], the aspect ratio α was defined as the ratio of the channel bottom width to the channel height. The comparison demonstrated good agreement with the experimental findings, as shown in Fig. 5.

The numerical values of the Nusselt number for double-trapezoidal (hexagonal) microchannels in the continuum flow regime were compared with the data presented by Shah and London [31]. As shown in Table 1, the agreement between the present results and the reference data is satisfactory.

The numerical values of the Nusselt number for rhombic microchannels in the continuum flow regime were compared with data presented by Shah and London [31] and by Saha et al. [37]. As shown in

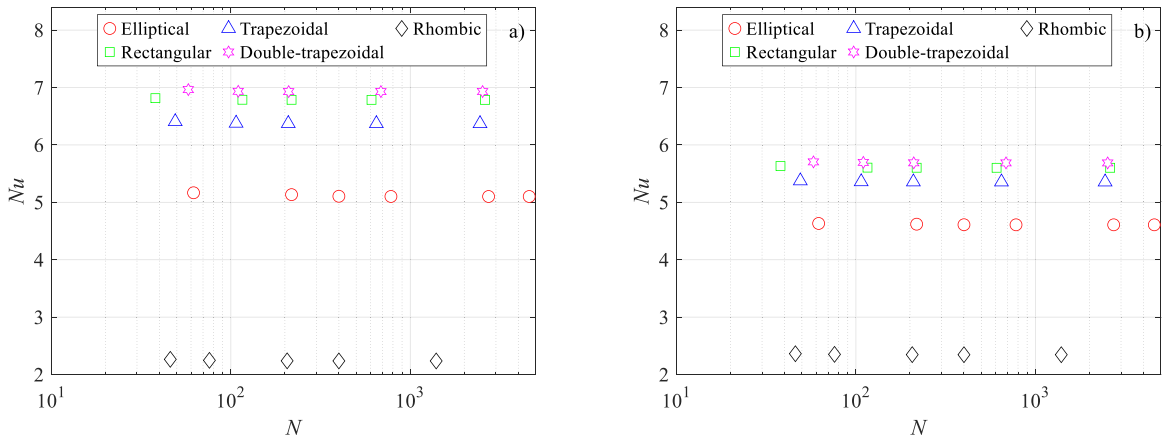

Fig. 3. Results of mesh independence analysis in terms of Nusselt numbers for all the investigated cross-sections with $\gamma = 0.1$: a) $L_s^*= 0$; b) $L_s^*= 0.05$.

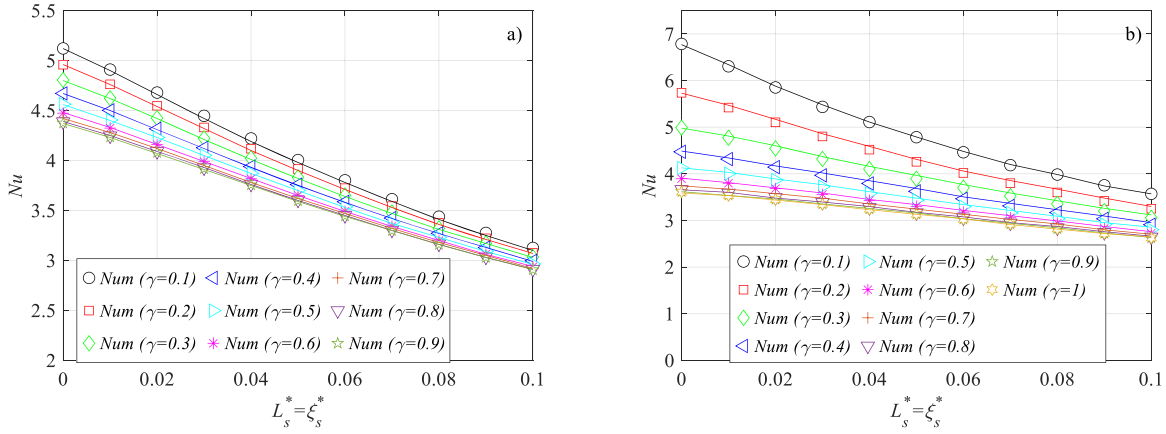

Fig. 4. Comparison of the Nusselt numbers with published data: a) elliptical microchannels (the lines depict the analytical solutions presented in [34]); b) rectangular microchannels (the lines depict the analytical solutions presented in [35]).

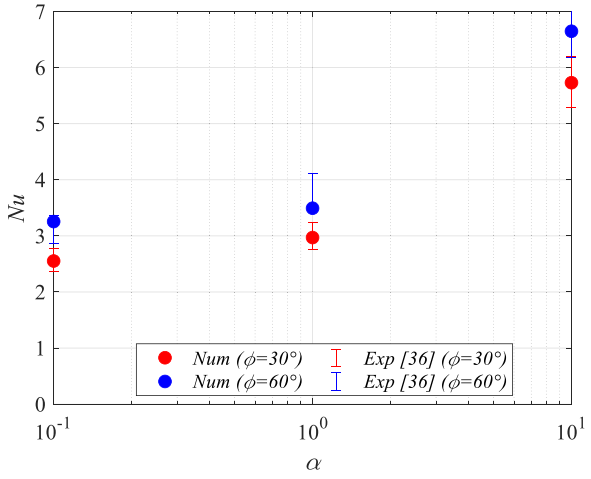

Fig. 5. Comparison of the Nusselt number for trapezoidal microchannels in continuum flow regime ($L^*_s = 0$) with the experimental data of Kewalramani et al. [36].

Table 1
Comparison of the Nusselt number for double-trapezoidal (hexagonal) microchannels with published data [31] (i.e., for $\gamma = 0.866$, $\varphi= 60°$ and $L_S^* = \xi_S^* = 0$).

Nu	*Nu* [31]	Difference
3.0019	3.002	−0.002 %

Table 2
Comparison of the Nusselt number for rhombic microchannels with published data [31,37].

φ[°]	*Nu*	*Nu* [37]	Difference	*Nu* [31]	Difference
10	2.202	1.502	46.59 %	2.216	0.63 %
20	2.454	2.040	20.28 %	2.457	0.13 %
30	2.720	2.482	9.61 %	2.722	0.06 %
40	2.971	2.836	4.76 %	2.969	0.06 %
50	3.190	3.111	2.54 %	3.188	0.06 %
60	3.369	3.315	1.61 %	3.367	0.05 %
70	3.500	3.458	1.23 %	3.500	0.01 %
80	3.581	3.546	0.98 %	3.581	0.01 %
90	3.608	3.590	0.51 %	3.608	0.00 %

Table 2, the comparison demonstrated perfect agreement with the data from [31]. Additionally, good agreement was observed with the data from [37] for acute angles greater than 30°, while discrepancies became more pronounced for smaller acute angles ($\varphi \leq 30°$). It is worth noting that the authors of [37] also found a discrepancy between their results and the data reported in [31]. They attributed this discrepancy to the boundary conditions employed in their analysis, the H1 condition, which was implemented by applying a thin wall made of a highly conductive, anisotropic material. This setup resulted in a non-uniform temperature distribution, with a maximum circumferential variation of approximately 1.5 °C.

These comparisons validated the numerical procedures followed in this work.

3. Results and discussion

The numerical results presented in this section encompass various slip lengths, temperature jump coefficients, and several aspect ratios. The temperature jump coefficients were assumed to be equivalent to the slip lengths (i.e. L_s/ξ_s =1), which means that the micro- and nano-structures employed in the superhydrophobic walls were considered to be aligned parallel to the flow direction [18]. The ratio of L_s/ξ_s is influenced by factors such as surface morphology and channel structure. Although variations in L_s/ξ_s will alter the critical parameter's value, the conclusions regarding the cross-sectional comparisons remain applicable.

Numerical results were generated by considering L_S and ξ_S values ranging between 0 μm and 5 μm [17,20] (i.e., L_s^* and ξ_s^* range from 0 to 0.05). The aspect ratio (γ) ranged as follows: from 0.1 to 1 for rectangular, elliptical, and rhombic microchannels; from 0.1 to 0.707 for trapezoidal microchannels; and from 0.1 to 1.414 for double-trapezoidal microchannels. For a silicon microchannel, the aspect ratio was limited by a maximum value of tg(φ)/2, which is approximately 0.707 when φ = 54.74° for ⟨100⟩ silicon wafers in which microchannels are fabricated by chemical etching using a KOH solution. Similarly, the double-trapezoidal (or hexagonal) cross-sections considered in this study were formed by merging two trapezoidal microchannels fabricated on ⟨100⟩ silicon wafers, restricting the aspect ratio to a maximum of 1.414 when φ = 54.74°

The comparison between different cross-sections was conducted under two distinct scenarios while maintaining the same hydraulic diameter:

1. All microchannels share the same maximum cross-sectional width (W_{ch}).
2. All microchannels have the same cross-sectional area (A).

The comparison in both scenarios was conducted using the ratio between the Nusselt and the Poiseuille numbers (*Nu/(f Re)),* because this ratio represents a crucial factor for optimizing the thermohydraulic performance of the heat sinks, as discussed in the previous section.

Furthermore, to demonstrate the practical applicability of the numerical model used in this study, various cross-sections were evaluated in the context of a real micro heat sink application.

3.1. Comparison at the same maximum width of the cross-section

To ensure a consistent width, the aspect ratio of the cross-section must be adjusted accordingly. The results presented were obtained considering two values for the width of the cross-section: W_{ch} equal to twice the hydraulic diameter and W_{ch} equal to three times the hydraulic diameter (i.e. $W_{ch}^*=W_{ch}/D_h$=2.0 and $W_{ch}^*=W_{ch}/D_h$=3.0). Table 3 presents the required aspect ratios along with the dimensionless wetted perimeters and cross-sectional areas as a function of the cross sectional geometry and W_{ch}^*.

The thermohydraulic performance of each cross-section, evaluated at the same maximum width in terms of both the Nusselt number and the Poiseuille number, is presented in Table 4. It is important to highlight that although double-trapezoidal (hexagonal) microchannels exhibit Nusselt number values comparable to those of rectangular microchannels, they offer a smaller convective heat transfer area due to their smaller wetted perimeter.

Furthermore, it was observed that rhombic cross-sections exhibit the lowest values for both Nusselt and Poiseuille numbers, attributed to the presence of sharp corners.

As indicated by Eq. (15), to optimize the thermal-hydraulic behavior of the heat sink by taking into account variations in pressure drop and convective heat transfer coefficient, the comparison among cross-sectional geometries must be conducted using the ratio of the Nusselt number to the Poiseuille number (*Nu/(f Re)*).

Fig. 6 compares the thermohydraulic performance of different microchannels based on the ratio *Nu/(f Re)*. It is worth noting that for both maximum cross-section width values considered in this study, the

Table 4
Thermohydraulic performance of the elliptical microchannels at the same maximum width of the cross-section.

Elliptical				
L_s (ξ_s)	*Nu*		*f Re*	
	W_{ch}^*=2.0	W_{ch}^*=3.0	W_{ch}^*=2.0	W_{ch}^*=3.0
0	4.72	4.92	17.52	18.42
0.025	4.58	4.76	14.22	14.75
0.05	4.33	4.47	11.97	12.31
Rectangular				
L_s (ξ_s)	*Nu*		*f Re*	
	W_{ch}^*=2.0	W_{ch}^*=3.0	W_{ch}^*=2.0	W_{ch}^*=3.0
0	4.79	5.74	17.08	19.07
0.025	4.62	5.40	13.83	15.18
0.05	4.34	4.96	11.64	12.63
Trapezoidal				
L_s (ξ_s)	*Nu*		*f Re*	
	W_{ch}^*=2.0	W_{ch}^*=3.0	W_{ch}^*=2.0	W_{ch}^*=3.0
0	3.32	4.75	13.80	17.13
0.025	3.34	4.58	11.50	13.83
0.05	3.27	4.31	9.87	11.61
Double-trapezoidal				
L_s (ξ_s)	*Nu*		*f Re*	
	W_{ch}^*=2.0	W_{ch}^*=3.0	W_{ch}^*=2.0	W_{ch}^*=3.0
0	4.95	5.93	17.52	19.58
0.025	4.76	5.55	14.19	15.57
0.05	4.46	5.08	11.95	12.93
Rhombic				
L_s (ξ_s)	*Nu*		*f Re*	
	W_{ch}^*=2.0	W_{ch}^*=3.0	W_{ch}^*=2.0	W_{ch}^*=3.0
0	2.69	2.43	12.78	12.42
0.025	2.76	2.51	10.66	10.35
0.05	2.75	2.52	9.15	8.88

Table 3
Geometrical properties of investigated cross-sections at the same maximum width of the cross-section.

Geometry	γ		P^*		A*	
	W_{ch}^*=2.0	W_{ch}^*=3.0	W_{ch}^*=2.0	W_{ch}^*=3.0	W_{ch}^*=2.0	W_{ch}^*=3.0
Elliptical	0.36	0.23	4.51	6.37	1.13	1.59
Rectangular	0.33	0.20	5.33	7.20	1.33	1.80
Trapezoidal	0.46	0.22	4.94	6.68	1.23	1.67
Double-trapezoidal	0.33	0.20	4.68	6.60	1.17	1.65
Rhombic	0.26	0.17	8.25	12.16	2.06	3.04

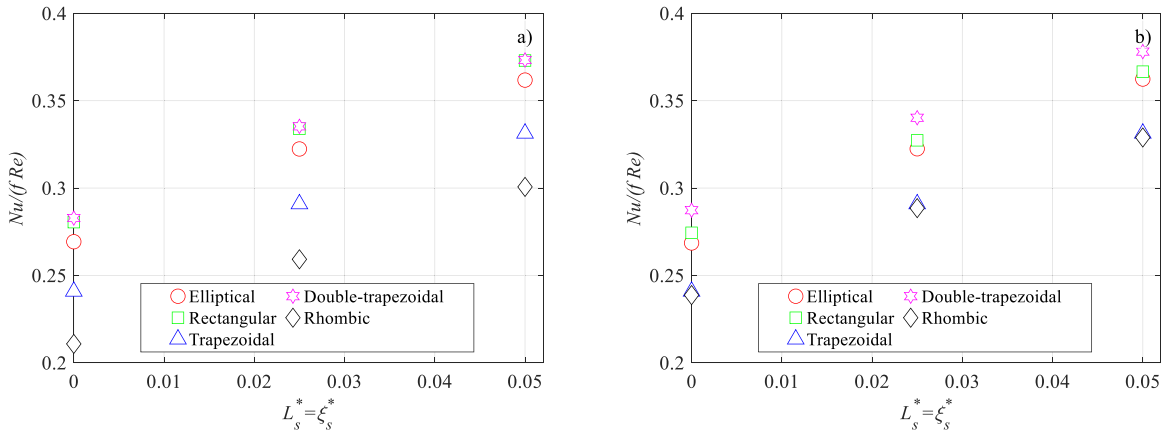

Fig. 6. Thermohydraulic performance of different cross-sections at the same maximum width: a) W_{ch}*= 2.0; b) W_{ch}*=3.0.

rectangular and double-trapezoidal (hexagonal) cross-sections exhibit the highest values of the ratio *Nu/(f Re)*, while the rhombus cross-section has the lowest. The elliptical and trapezoidal cross-sections fall between these two. Similar findings were reported by Alfaryjat et al. [8], who compared the performance of hexagonal, circular, and rhombus cross-section micro heat sinks in the continuum regime.

Additionally, it is noteworthy that *Nu/(f Re)* increases with the growing impact of the slip, indicating that the reduction in the Nusselt number due to slip effects is less important than the reduction in the *f Re* product. The reduction in hydraulic diameter, while maintaining a fixed maximum width, leads to an increase in *Nu/(f Re)*, as demonstrated by the comparison between Figs. 6a and 6b.

The impact of slip on the thermohydraulic performance of the microchannels studied is more clearly illustrated in Fig. 7, which highlights the increase in *Nu/(f Re)* for L_s=ξ_s =0.05, with respect to the baseline case with no-slip and no-temperature-jump conditions. It can be observed that the impact of the slip is very significant for each cross-section geometry. Thus, it was confirmed that the slip effect reduces frictional resistance in the fluid, leading to an increase in the thermohydraulic performance of the MCHS. In particular, the rhombic microchannels exhibit the highest increase in *Nu/(f Re)* while the double-trapezoidal (hexagonal) channels exhibit the lowest ones for both values of the maximum width considered in the present analysis.

3.2. Comparison at the same cross-sectional area

In the presented results, the cross-sectional area was defined as 1.24 times and 2.66 times the squared hydraulic diameter, respectively (i.e. A^*= 1.24 and A^*= 2.66). These values were chosen by considering the particular trapezoidal cross-section investigated in this study (i.e., the KOH-etched trapezoidal microchannel).

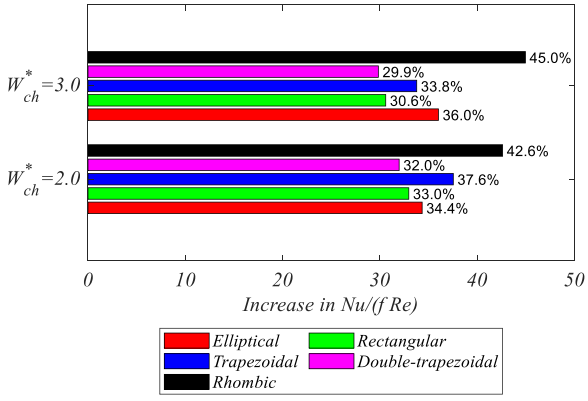

Fig. 7. Effect of the slip on the thermohydraulic performance of different cross-sections at the same maximum width (L_s = ξ_s = 0.05). The *x*-axis represents incremental changes relative to the baseline case with no-slip and no-temperature-jump conditions.

Table 5 presents the required aspect ratios, along with the dimensionless wetted perimeters. It is important to note that maintaining the same cross-sectional area and hydraulic diameter preserves the wetted perimeter, thereby ensuring the same convective heat transfer area (i.e., the same heat transfer rate).

The thermohydraulic performance of each cross-section, evaluated at the same cross-sectional area in terms of both the Nusselt number and the Poiseuille number, is presented in Table 6. In this scenario, the trapezoidal and rhombic cross-sections exhibited similar performance. It is important to highlight that maintaining the same wetted perimeter ensures an identical convective heat transfer area. As a result, cross-sections with the highest Nusselt number correspond to the lowest temperature difference.

The thermohydraulic performance of the various microchannels is compared in Fig. 8 in terms of the ratio *Nu/(f Re)*. The results revealed that for the smallest cross-sectional area examined, double-trapezoidal (hexagonal) microchannels demonstrated the highest performance. In contrast, for the largest cross-sectional area, both rectangular and double-trapezoidal (hexagonal) microchannels exhibit equivalent performance levels.

A comparison between Fig. 8a and 8b clearly shows that increasing the cross-sectional area while maintaining a fixed hydraulic diameter leads to an increase in *Nu/(f Re)*.

Fig. 9 shows the increase in *Nu/(f Re)* for L_s=ξ_s =0.05, with respect to the baseline case with no-slip and no-temperature-jump conditions. Notably, rhombic microchannels exhibit the greatest increase in *Nu/(f Re)*, while double-trapezoidal (hexagonal) channels show the smallest increase, even at the same cross-sectional area.

3.3. Application of the numerical model to a real micro heat sink

The microchannel heat sink examined in this section consists of parallel, straight channels made from silicon, with width (*W*), height (*H*), and length (*L*) dimensions measuring 5 cm, 0.4 cm, and 5 cm,

Table 5
Geometrical properties of investigated cross-sections at the same cross-sectional.

Geometry	*γ*		*P**	
	A^*= 1.24	A^*= 2.66	A^*= 1.24	A^*= 2.66
Elliptical	0.31	0.13	4.97	10.59
Rectangular	0.39	0.12	4.97	10.59
Trapezoidal	0.46	0.12	4.94	10.63
Double-trapezoidal	0.30	0.11	4.98	10.65
Rhombic	0.50	0.20	4.97	10.59

Table 6
Thermohydraulic performance of the elliptical microchannels at the same cross-sectional area.

Elliptical				
L_s (ξ_s)	*Nu*		*f Re*	
	A^*= 1.24	A^*= 2.66	A^*= 1.24	A^*= 2.66
0	4.79	5.08	17.82	19.13
0.025	4.64	4.90	14.39	15.19
0.05	4.38	4.59	12.08	12.60
Rectangular				
L_s (ξ_s)	*Nu*		*f Re*	
	A^*= 1.24	A^*= 2.66	A^*= 1.24	A^*= 2.66
0	4.52	6.57	16.49	20.74
0.025	4.39	6.06	13.42	16.31
0.05	4.16	5.47	11.34	13.45
Trapezoidal				
L_s (ξ_s)	*Nu*		*f Re*	
	A^*= 1.24	A^*= 2.66	A^*= 1.24	A^*= 2.66
0	3.32	6.13	13.80	20.08
0.025	3.34	5.71	11.50	15.87
0.05	3.27	5.21	9.87	13.13
Double-trapezoidal				
L_s (ξ_s)	*Nu*		*f Re*	
	A^*= 1.24	A^*= 2.66	A^*= 1.24	A^*= 2.66
0	5.15	6.83	17.93	21.43
0.025	4.92	6.25	14.46	16.80
0.05	4.59	5.63	12.14	13.83
Rhombic				
L_s (ξ_s)	*Nu*		*f Re*	
	A^*= 1.24	A^*= 2.66	A^*= 1.24	A^*= 2.66
0	3.26	2.51	13.65	12.53
0.025	3.29	2.59	11.39	10.44
0.05	3.22	2.59	9.79	8.96

respectively. Water is used as the cooling fluid. The detailed dimensions are presented in Table 7, where N_{ch} indicate the number of microchannels for each investigated cross-section.

The cross-sections shown in Fig. 2 were utilized to assess the thermohydraulic performance of the micro heat sinks. The comparison of different cross-sections was conducted under the assumption that all microchannels had the same cross-sectional area (A), ensuring an identical heat transfer area across all configurations.

To apply the numerical model used in this study to a real micro heat sink, it was essential to validate the assumptions underlying the derivation of the governing equations. To validate the assumption regarding the thermophysical properties of the working fluid, it was necessary to evaluate the increase in the fluid bulk temperature. Given the operating conditions outlined in Table 8, the temperature increase of water from the inlet to the outlet was <5 °C, resulting in minimal changes to the fluid properties.

To confirm the assumption of a fully developed flow, the lengths of the dynamic and thermal entry regions were evaluated. These entrance lengths within the continuum flow regime were estimated by means of established correlations found in the literature [37–41]. The hydrodynamic entrance length could only be determined for circular [42], rectangular [43,44], and square [45]. Based on the geometric properties of the investigated cross-sections shown in Table 7 and the operating

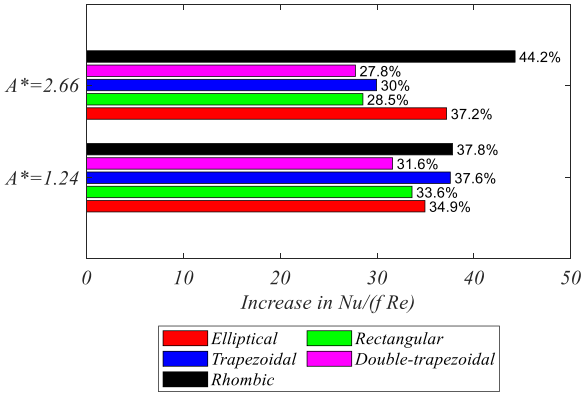

Fig. 9. Effect of the slip on the thermohydraulic performance of different cross-sections at the same cross-sectional area ($L_s = \xi_s = 0.05$). The x-axis represents incremental changes relative to the baseline case with no-slip and no-temperature-jump conditions.

Table 7
Geometrical properties of investigated cross-sections at the same cross-sectional area (A^*= 1.24).

	Geometry				
	Elliptical	Rectangular	Trapezoidal	Double-trapezoidal	Rhombic
W_{ch} (μm)	226	179	200	216	222
W_U (μm)	626	579	600	616	622
H_{ch} (μm)	70	69	92	65	112
γ	0.31	0.39	0.46	0.30	0.50
N_{ch}	79	86	83	81	80

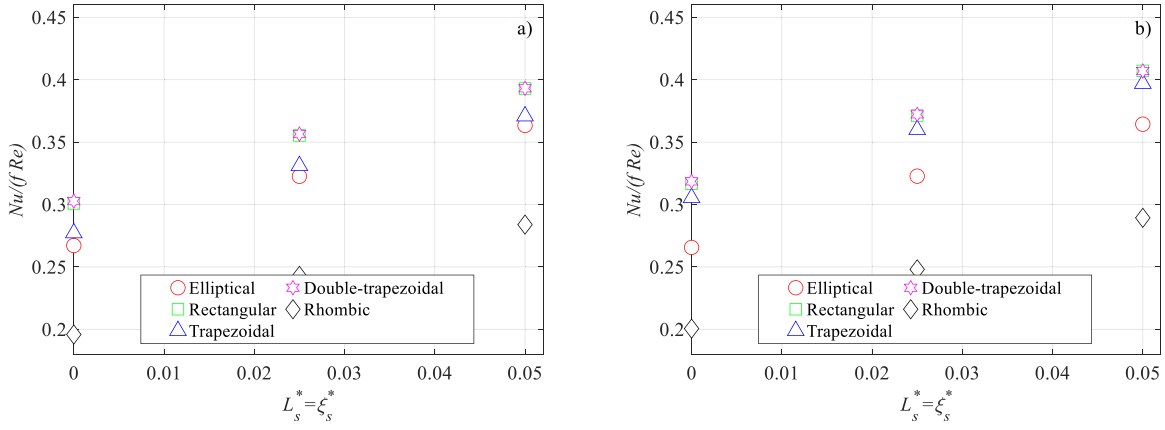

Fig. 8. Thermohydraulic performance of different cross-sections at the same cross-sectional area: a) A^*= 1.24; b) A^*= 2.66.

Table 8
Operating conditions.

Variable	*Value range*
Reynolds number	800
Prandtl number	5.84
Slip length (μm)	0–5
Temperature jump (μm)	0–5
Applied heat flux (W cm^{-2})	5

conditions detailed in Table 8, the thermal entrance lengths in the continuum flow regime were 1.1 cm, 2.9 cm, 2.9 cm, 2.8 cm, and 3.7 cm for the elliptical, rectangular, trapezoidal, double-trapezoidal (hexagonal), and rhombic cross-sections, respectively.

Regarding the assumption of negligible axial conduction, it is important to note that as the Peclet number increases, the influence of axial heat conduction gradually diminishes until convective heat transfer fully dominates [46]. Furthermore, an evaluation of the parameter proposed by Lin et al. [47] to quantify the impact of axial heat conduction on channel walls confirmed that, under the micro heat sink and operating conditions considered in this study, axial conduction was negligible.

Once the accuracy of the mathematical model was confirmed, the thermohydraulic performance of the MCHS was assessed. The total thermal resistance values for the investigated micro heat sink, evaluated by sing Eq. (11), are summarized in Table 9. It is important to highlight that the conductive thermal resistances remain the same, while the fluid thermal resistances remain unchanged due to the consistent flow rate. However, the convective thermal resistance for $\xi_s^* = 0.05$ is higher than that for $\xi_s^* = 0$, as the corresponding convective heat transfer coefficient for $\xi_s^* = 0.05$ is lower than that for $\xi_s^* = 0$. Therefore, the thermohydraulic performance of micro heat sinks with superhydrophobic walls is lower than that of those with conventional walls under identical flow rate conditions. These same findings were highlighted by Gong et al. [20]. Additionally, Ermagan and Rafee [19] highlighted that at higher pumping power levels, the use of superhydrophobic walls leads to a deterioration in the thermal performance of microchannels.

When comparing the cross-sections, it is evident that the rectangular and double-trapezoidal shapes also demonstrate the best thermohydraulic performance in a real micro heat sink.

The values of the pumping power required by the investigated micro heat sink, evaluated by sing Eq. (13), are summarized in Table 10. It can be observed that the induced slip velocity and the resulting drag reduction led to a significant decrease in pumping power. The maximum reduction in pumping power is about 32 % for $\xi_s^* = 0.05$. It is evident that the rectangular and double-trapezoidal shapes also demonstrate the best performance in terms of pumping power.

4. Conclusions

In this study, the thermohydraulic performance of laminar flow in microchannels with rectangular, trapezoidal, double-trapezoidal, elliptical, and rhombic cross-sections, taking into account slip velocity and temperature jump at the wall, were compared. The heat transfer analysis assumes a constant heat transfer rate along the axial direction and a uniform wall temperature around the cross-section perimeter, which corresponds to the H1 boundary condition. This condition is particularly relevant for microchannels subjected to imposed heat fluxes and made with high thermal conductivity materials (i.e., silicon wafers, metals, and so on).

Table 9
Total thermal resistance of the investigated micro heat sink [K/W].

	Geometry				
ξ_s^*	Elliptical	Rectangular	Trapezoidal	Double-trapezoidal	Rhombic
0	0.0529	0.0496	0.0579	0.0503	0.0603
0.025	0.0535	0.0501	0.0577	0.0510	0.0601
0.05	0.0545	0.0511	0.0583	0.0522	0.0606

Table 10
Pumping power of the investigated micro heat sink [W].

	Geometry				
ξ_s^*	Elliptical	Rectangular	Trapezoidal	Double-trapezoidal	Rhombic
0	7.04	7.08	5.66	7.23	5.46
0.025	5.69	5.77	4.71	5.83	4.56
0.05	4.77	4.87	4.05	4.90	3.92

The numerical results reveal that slip effects significantly impact all cross-sectional geometries. In particular, the introduction of slip reduces fluid friction, leading to a notable decrease in the pumping power. However, the analysis also shows that micro heat sinks with superhydrophobic walls have lower thermal performance compared to those with conventional (no-slip) walls when operated at the same flow rate. Interestingly, the ratio between the Nusselt and the Poiseuille numbers increases as slip effects become more pronounced, suggesting that the decrease in heat transfer (Nusselt number) due to slip is outweighed by the greater reduction in the frictional resistance ($f\,Re$ product).

The key findings of the analysis are summarized as follows:

- For both maximum cross-sectional width values considered in this study, the rectangular and double-trapezoidal (hexagonal) cross-sections showed the highest thermohydraulic performance, while the rhombic cross-section exhibited the lowest. The elliptical and trapezoidal cross-sections fall between these two extremes.
- For the smallest cross-sectional area examined, double-trapezoidal (hexagonal) microchannels demonstrated the highest thermohydraulic performance at the same cross-sectional area.
- For the largest cross-sectional area, rectangular and double-trapezoidal (hexagonal) microchannels exhibited comparable thermohydraulic performance under identical conditions.
- The rhombic microchannels are the most sensitive to slip effects, while the double-trapezoidal ones are the least sensitive.

Despite the assumptions made, the numerical model used in this study offers benchmark results that are valuable for validating both approximate and computational alternative approaches.

Future research will investigate the impact of the ratio between slip length and temperature jump coefficient on the thermohydraulic performance of microchannel heat sinks. Additionally, the relationship between surface morphology—particularly as influenced by superhydrophobic treatments—and slip length will be examined experimentally.

Nomenclature

A	Cross section area, m^2
A^*	Non-dimensional cross section area
W_{ch}	Maximum width of the cross-section, m
H_{ch}	Height of the cross-section, m
c_p	Specific heat at constant pressure, J/(kg•K)
D_h	Hydraulic diameter of the channel, m
f	Fanning friction factor
$f\,Re$	Poiseuille number
h	Convective heat transfer coefficient, W(m^2•K)
k	Specific heat ratio c_p/c_v
Kn	Knudsen number, d_g/D_h
L	Length, m
n^*	Non-dimensional normal to the wall
N	Number of finite elements
Nu	Nusselt number, hD_h/λ
P	Perimeter of the cross-section, m

(*continued on next page*)

(*continued*)

P^*	Non-dimensional perimeter of the cross-section
p	Fluid pressure, Pa
p^*	Non-dimensional fluid pressure
Pe	Peclet number
Pr	Prandtl number
q'	Thermal power per unit of length, W/m
R	Thermal resistance, K/W
R^*	Non-dimensional thermal resistance
Re	Reynolds number
T	Fluid temperature, K
v	Fluid velocity, m/s
v^*	Non-dimensional fluid velocity
$\overline{v}$	Average fluid velocity, m/s
$\dot{V}$	Volumetric flow rate, m^3/s
x,y,z	Cartesian coordinates, m
x^*,y^*,z^*	Non-dimensional Cartesian coordinates
Greek symbols	
Δp	Pressure drop, Pa
γ	Aspect ratio, H_{ch} / W_{ch}
T^*	Non-dimensional fluid temperature
λ	Fluid thermal conductivity, W/(m•K)
μ	Fluid dynamic viscosity, Pa•s
ξ_s	Temperature jump coefficient, m
$\xi_s{}^*$	Non-dimensional temperature jump coefficient
ρ	Fluid density, kg/m^3
Ω	Pumping power, W
Ω^*	Non-dimensional pumping power
Subscripts	
b	bulk
$cond$	conductive
$conv$	convective
f	fluid
s	slip
tot	total
w	wall

CRediT authorship contribution statement

Pamela Vocale: Writing – original draft, Methodology, Investigation, Funding acquisition, Formal analysis, Conceptualization. **Gian Luca Morini:** Writing – review & editing, Supervision.

Declaration of competing interest

The authors declare that they have no known competing financial interests or personal relationships that could have appeared to influence the work reported in this paper.

Acknowledgments

This research was funded under the National Recovery and Resilience Plan (NRRP), Mission 4 Component 2 Investment 1.5—Call for tender No 3277 of 30/12/2021 of Italian Ministry of University and Research funded by the European Union—NextGenerationEU. Award Number: Project code ECS00000033, Concession Decree No 1052 of 23/06/2022 adopted by the Italian Ministry of University and Research, CUP D93C22000460001, "Ecosystem for Sustainable Transition in Emilia-Romagna" (Ecosister).

Data availability

Data will be made available on request.

References

[1] M. Harris, et al., Overview of recent trends in microchannels for heat transfer and thermal management applications, Chem. Eng. Process. Process Intensif. 181 (2022) 109155.
[2] W. Dong, et al., Research progress on passive enhanced heat transfer technology in microchannel heat sink, Int. J. Heat Mass Transf. 220 (2024) 125001.
[3] Z. He, Y. Yan, Z. Zhang, Thermal management and temperature uniformity enhancement of electronic devices by micro heat sinks: a review, Energy 216 (2021) 119223.
[4] Y. Chen, et al., Three-dimensional numerical simulation of heat and fluid flow in noncircular microchannel heat sinks, Int. Commun. Heat Mass 36 (2009) 917–920.
[5] P. Gunnasegaran, et al., The effect of geometrical parameters on heat transfer characteristics of microchannels heat sink with different shapes, Int. Commun. Heat Mass Transf. 37 (2010) 1078–1086.
[6] P. Canhoto, A.H. Reis, Optimization of forced convection heat sinks with pumping power requirements, Int. J. Heat Mass Transf. 54 (2011) 1441–1447.
[7] M.R. Salimpour, M. Sharifhasan, E. Shirani, Constructal optimization of microchannel heat sinks with noncircular cross sections, Heat Transf. Eng. 34 (2013) 863–8749.
[8] A.A. Alfaryjat, et al., Influence of geometrical parameters of hexagonal, circular, and rhombus microchannel heat sinks on the thermohydraulic characteristics, Int. Commun. Heat Mass Transfer 52 (2014) 121–131.
[9] H. Wang, Z. Chen, J. Gao, Influence of geometric parameters on flow and heat transfer performance of micro-channel heat sinks, Appl. Therm. Eng. 107 (2016) 870–879.
[10] D. Jing, L. He, Numerical studies on the hydraulic and thermal performances of microchannels with different cross-sectional shapes, Int. J. Heat Mass Tran. 143 (2019) 118604.
[11] C. Ybert, et al., Achieving large slip with superhydrophobic surfaces: scaling laws for generic geometries, Phys. Fluids 19 (2007) 123601.
[12] G. Rosengarten, J. Cooper-White, G. Metcalfe, Experimental and analytical study of the effect of contact angle on liquid convective heat transfer in microchannels, Int. J. Heat Mass Transf. 49 (2006) 4161–4170.
[13] G. Karniadakis, A. Beskok, N. Aluru, Microflows and Nanoflows - Fundamentals and Simulation, Springer, New York, 2005.
[14] C. Carotenuto, et al., Predicting the apparent wall slip when using roughened geometries: a porous medium approach, J. Rheol. 59 (2015) 1131–1149.
[15] M. Del Mastro, A. Terzis, On the exact solutions of Darcy–Brinkman model in rectangular Hele–Shaw channels under no-slip and slip boundary conditions, Phys. Fluids 37 (2025) 032005.
[16] M.R. Hajmohammadi, P. Alipour, H. Parsa, Microfluidic effects on the heat transfer enhancement and optimal design of microchannels heat sinks, Int. J. Heat Mass Transf. 126 (2018) 808–815.
[17] H. Ermagan, R. Rafee, Numerical investigation into the thermo-fluid performance of wavy microchannels with superhydrophobic walls, Int. J. Thermal Sci. 132 (2018) 578–588.
[18] H. Ermagan, R. Rafee, Geometric optimization of an enhanced microchannel heat sink with superhydrophobic walls, Appl. Therm. Eng. 130 (2018) 384–394.
[19] H. Ermagan, R. Rafee, Effect of pumping power on the thermal design of converging microchannels with superhydrophobic walls, Int. J. Thermal Sci. 132 (2018) 104–116.
[20] W. Gong, et al., Thermal-hydraulic performance enhancement analysis of microtube with superhydrophobic surfaces, Int. J. Heat Mass Transf. 144 (2019) 118697.
[21] A. Joy, K.V. Shiblemon, B. Baby, Review on fabrication and experimental study of microchannel heat sinks for cooling of electronic components, Mater. Today: Proc. 72 (2023) 2985–2991.
[22] H. Zhou, et al., All laser-based fabrication of microchannel heat sink, Mater. Des. 221 (2022) 110968.
[23] M. Tilli, et al., Handbook of Silicon Based MEMS Materials and Technologies, 2nd Edition, Elsevier Inc.: Amsterdam, 2015.
[24] S.A. Kumar, et al., A review on additive manufacturing of topology optimized microchannel heat sink, Heat Transf. Eng. (2025).
[25] H.D.M. Hettiarachchi, et al., Numerical simulation of wall roughness on gaseous flow and heat transfer in a microchannel, Int. J. Heat Mass Transf. 49 (2006) 1329–1339.
[26] C.L.M.H. Navier, Mémoire sur les lois dy movement des fluids, Mem. Acad. R. Sci. Inst. Fr. 6 (1827) 389–440.
[27] D.C. Tretheway, C.D. Meinhart, Apparent fluid slip at hydrophobic microchannel walls, Phys. Fluids 14 (2002) L9–L12.
[28] D. Maynes, J. Crockett, Apparent temperature jump and thermal transport in channels with streamwise rib and cavity featured superhydrophobic walls at constant heat flux, J. Heat Transf. 136 (2014) 011701.
[29] A. Cowley, D. Maynes, J. Crockett, Effective temperature jump length and influence of axial conduction for thermal transport in superhydrophobic channels, Int. J. Heat Mass Transf. 79 (2014) 573–583.
[30] D. Maynes, et al., Analysis of laminar slip-flow thermal transport in microchannels with transverse rib and cavity structured superhydrophobic walls at constant heat flux, J. Heat Transf. 135 (2013) 021701.
[31] R.K. Shah, A.L. London, Laminar Flow Forced Convection in Ducts, Academic Press, New York, 1978.
[32] T.-C. Hung, W.-M. Yan, Optimization of a microchannel heat sink with varying channel heights and widths, Numer. Heat Transf. Part A: Appl. Int. J. Comput. Methodol. 62 (2012) 722–741.
[33] COMSOL Multiphysics. 2023. Reference Manual.
[34] L. Su, et al., Analytical solutions of slip flow and H1 heat transfer in elliptical microchannels, Int. J. Thermal Sci. 184 (2023) 108017.
[35] L. Ghodoossi, N. Eğrican, Prediction of heat transfer characteristics in rectangular microchannels for slip flow regime and H1 boundary condition, Int. J. Thermal Sci. 44 (2005) 513–520.

[36] G.V. Kewalramani, G. Hedau, S.K. Saha, A. Agrawal, Empirical correlation of laminar forced convective flow in trapezoidal microchannel based on experimental and 3D numerical study, Int. J. Thermal Sci. 142 (2019) 422–433.
[37] S.K. Saha, A. Agrawal, Y. Soni, Heat transfer characterization of rhombic microchannel for H1 and H2 boundary conditions, Int. J. Thermal Sci. 111 (2017) 223–233.
[38] L. Su, et a. Laminar flow and heat transfer in the entrance region of elliptical minichannels, Int. J. Heat Mass Transf. 145 (2019) 118717.
[39] P.-S. Lee, S.V. Garimella, Thermally developing flow and heat transfer in rectangular microchannels of different aspect ratios, Int. J. Heat Mass Transf. 49 (2006) 3060–3067.
[40] J.P. McHale, S.V. Garimella, Heat transfer in trapezoidal microchannels of various aspect ratios, Int. J. Heat Mass Transf. 53 (2010) 365–375.
[41] M. Iwaniszyn, et al., Entrance effects on forced convective heat transfer in laminar flow through short hexagonal channels: experimental and CFD study, Chem. Eng. J. 405 (2021) 126635.
[42] Z. Duan, Y.S. Muzychka, Slip flow in the hydrodynamic entrance region of circular and noncircular microchannels, J. Fluids Eng. 132 (2010), 011201-1.
[43] N. Ma, et al., Lattice Boltzmann simulation of the hydrodynamic entrance region of rectangular microchannels in the slip regime, Micromachines 9 (2018) 87.
[44] S.S. Hsieh, C.Y. Lin, Convective heat transfer in liquid microchannels with hydrophobic and hydrophilic surfaces, Int. J. Heat Mass Transf. 52 (2009) 260–270.
[45] W. Gong, et al., Effects of slip length and hydraulic diameter on hydraulic entrance length of microchannels with superhydrophobic surfaces, Front. Energy 14 (2020) 127–138.
[46] J. Zhang, Z. Zou, C. Fu, A review of the complex flow and heat transfer characteristics in microchannels, Micromachines 14 (2023) 1451.
[47] T.-Y. Lin, S.G. Kandlikar, A theoretical model for axial heat conduction effects during single-phase flow in microchannels, J. Heat Transf. 134 (2012) 020902.